ACS NANO

www.acsnano.org

ARTICLE

Density Matching Multi-wavelength Analytical Ultracentrifugation to Measure Drug Loading of Lipid Nanoparticle Formulations

Amy Henrickson, Jayesh A. Kulkarni, Josh Zaifman, Gary E. Gorbet, Pieter R. Cullis, and Borries Demeler*

Cite This: *ACS Nano* 2021, 15, 5068−5076

Read Online

ACCESS | Metrics & More | Article Recommendations | Supporting Information

ABSTRACT: **Previous work suggested that lipid nanoparticle (LNP) formulations, encapsulating nucleic acids, display electron-dense morphology when examined by cryogenic-transmission electron microscopy (cryo-TEM). Critically, the employed cryo-TEM method cannot differentiate between loaded and empty LNP formulations. Clinically relevant formulations contain high lipid-to-nucleic acid ratios (10−25 (w/w)), and for systems that contain mRNA or DNA, it is anticipated that a substantial fraction of the LNP population does not contain a payload. Here, we present a method based on the global analysis of multi-wavelength sedimentation velocity analytical ultracentrifugation, using density matching with heavy water, that not only measures the standard sedimentation and diffusion coefficient distributions of LNP mixtures, but also reports the corresponding partial specific volume distributions and optically separates signal contributions from nucleic acid cargo and lipid shell. This makes it possible to reliably predict molar mass and anisotropy distributions, in particular, for systems that are heterogeneous in partial specific volume and have low to intermediate densities. Our method makes it possible to unambiguously measure the density of nanoparticles and is motivated by the need to characterize the extent to which lipid nanoparticles are loaded with nucleic acid cargoes. Since the densities of nucleic acids and lipids substantially differ, the measured density is directly proportional to the loading of nanoparticles. Hence, different loading levels will produce particles with variable density and partial specific volume. An UltraScan software module was developed to implement this approach for routine analysis.**

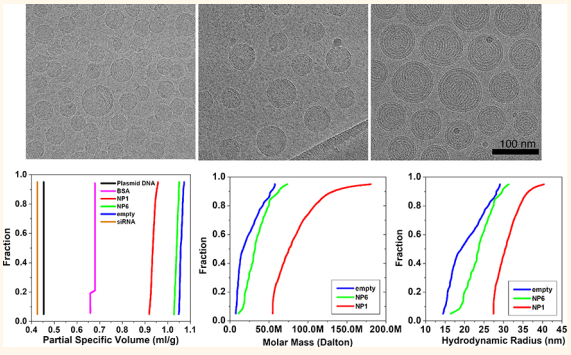

KEYWORDS: *lipid nanoparticles, multi-wavelength analytical ultracentrifugation, density matching, RNA gene therapy, nanomedicine, lipid biophysics, loading heterogeneity*

INTRODUCTION

Analytical ultracentrifugation (AUC) is a solution-based separation technique with nearly a century of applications in biomolecular research. It is a first principles technique which does not require external standards and is considered the gold standard for studying the composition and interactions of colloidal biopolymers, nanomaterials, and synthetic polymers and has recently seen significant advances in instrumentation and analysis software.[1−11] During sedimentation velocity experiments (SVEs), centrifugal forces create moving concentration gradients, and their evolution over time and space are monitored by either their absorbance at one or more wavelengths,[6] their fluorescence emission (if the molecules contain fluorophores), or their refractive index changes, using Rayleigh interference. Mass transport of the solutes occurs through both sedimentation and diffusion. Both transport processes are impacted by the frictional properties of the molecules and the viscosity of the solvent through molecular surface−solvent interactions. Sedimentation transport also depends on the mass of the sedimenting particles, their partial specific volumes (PSVs), and the density of the solvent. All experimental data can be directly fitted to finite element solutions of partial differential equations,[12,13] providing hydrodynamic details such as sedimentation and diffusion coefficients, as well as partial concentrations of analytes present

Received: December 1, 2020
Accepted: February 17, 2021
Published: February 22, 2021

https://dx.doi.org/10.1021/acsnano.0c10069
ACS Nano 2021, 15, 5068−5076

in mixtures. Sedimentation and diffusion coefficients can further be interpreted to derive anisotropy, density, and molar mass, as well as thermodynamic interaction parameters when studying mass action effects. In this study, we employ SVEs performed in multi-wavelength mode (MW-AUC),[14−16] coupled to density matching with heavy water, to characterize the loading of lipid nanoparticles (LNPs).[17]

LNPs represent a mature drug-delivery technology that enable the therapeutic potential of nucleic acids. Onpattro, an RNA interference therapeutic approved by the U.S. Food and Drug Administration, uses LNPs to entrap short interfering RNA (siRNA), protects it from degradation during circulation, and enhances intracellular delivery into hepatocytes at the liver. These LNP-siRNA are approximately 50 nm in diameter[18] and are electron-dense when visualized by cryogenic-transmission electron microscopy (cryo-TEM).[19] A critical knowledge gap is the inability to differentiate between empty LNPs and those loaded with nucleic acid by using the same cryo-TEM technique. One exception is the use of formulations that contain completely charge-neutralized ionizable lipids where clear multilamellar structures are observed. Comparatively, clinically relevant LNP contain substantially higher amounts of ionizable lipid (amine-to-phosphate (N/P) ratios of 3−6), resulting in indistinguishable morphology between empty and partially loaded LNPs. Likewise, the interparticle distribution of siRNA cannot be easily determined. The presence of siRNA can be detected using spectrophotometric methods, but they do not differentiate loaded from free nucleic acid. Dynamic light scattering (DLS) provides information about the size of particles, but similarly sized LNPs containing nucleic acids cannot be resolved from those without cargo. Hence, such methods are unable to distinguish heterogeneity of loading and fail to distinguish empty from partially filled LNPs.

Determining the exact amount of nucleic acid that is loaded into an LNP poses a complicated challenge for several reasons: The self-assembly of these particles invariably leads to some heterogeneity in the particle size (even with low polydispersity indices of <0.1) and interparticle RNA copy number. Their physicochemical analyses are typically performed on bulk samples and represent an average of the population. Solution techniques such as dynamic light scattering and size exclusion chromatography have difficulties distinguishing between LNPs which are empty or partially or fully loaded with cargo due to limitations in resolution and separability. It is important to note that the two components in LNPs (lipid and nucleic acid) have very different densities. Nucleic acids are much denser than the lipid excipients, which include four components: an ionizable cationic lipid, phospholipid, cholesterol, and poly-(ethylene glycol) (PEG) lipid. The method presented here exploits this difference in density to estimate the loading amounts of LNPs by employing a MW-AUC approach that is based on density matching with heavy water. At the same time, this method leverages the spectral differences between a lipid nanostructure, which scatters light, and the nucleic acid cargo, which has a unique chromophore at ∼260 nm, to achieve optical separation, orthogonal to the hydrodynamic separation. As we demonstrate here, this method is ideally suited for the solution composition characterization of LNP preparations, which are inherently heterogeneous in size and loading. Unlike electron microscopy and single-molecule techniques, it provides high statistical certainty through bulk observation. A multi-wavelength detector offers differential detection of samples containing a mixture of analytes that vary in chemical composition. Our method is sensitive to all parameters of interest for LNP characterization and, by virtue of the extensions discussed here, successfully addresses the challenges posed by LNP formulation characterization.

RESULTS AND DISCUSSION

We investigated the loading of LNPs with siRNA by multi-wavelength AUC (MW-AUC) and density matching SVEs. Combining these two methods by global analysis produces orthogonal information, which enhances the confidence in the results obtained by either method alone and provides very high resolution and detail on particle size and cargo loading. To illustrate this approach, we compared LNP preparations containing siRNA to empty LNPs, free nucleic acid, and protein. To further validate the method, hydrodynamic radius (R_h) distributions obtained from MW-AUC were compared to those obtained by cryo-TEM and dynamic light scattering. Three key preparations are referenced in the following text: empty LNPs, and LNP-siRNA systems generated at a loading ratio of 1 or 6 molecules of ionizable cationic lipid for each nucleic acid phosphate, referred to as NP1 or NP6, respectively.

Analysis of Partial Specific Volume. Density variations in the LNP preparations are assessed by measuring their partial specific volume (PSV) using a density matching approach.[17] The PSV can be viewed as the inverse of the particle density of the hydrated, sedimenting particle. The PSV results for these LNP preparations, together with reference standards, including siRNA used for encapsulation, a 2.88kb double-stranded DNA fragment, and bovine serum albumin protein (BSA), are shown in Figure 1. In Figures 1−5, and Figure 9, we report

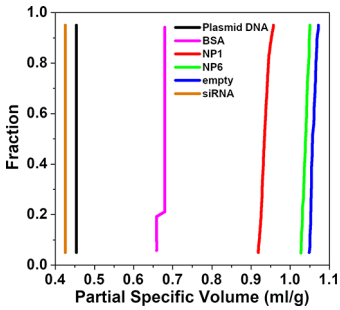

Figure 1. PSV distributions for pure 21 bp siRNA (brown), 2.88 kb linear double-stranded plasmid DNA (black), bovine serum albumin (BSA, magenta), NP1 (red), NP6 (green), and empty LNP (blue).

distributions using integral representations, which directly provide fractions of the total concentration on the *Y*-axis for different species. For example, in Figure 1, all of the plasmid DNA (black line) and siRNA exhibit the same PSV for all fractions, producing a vertical plot, which suggests homogeneity in PSV. BSA (magenta line) shows two discrete PSV values for monomer (0.68 mL/g, ∼80%) and dimer (0.66 mL/g, ∼20%), and LNPs (red, green, and blue lines) produce heterogeneous distributions, where each fraction relates to a different PSV value.

As expected, empty LNPs display the lowest density distribution (highest partial specific volume), with average PSV values of 1.06 mL/g, consistent with their flotation in light water. Empty LNPs are followed by NP6 LNPs, resulting in an

https://dx.doi.org/10.1021/acsnano.0c10069
ACS Nano 2021, 15, 5068−5076

average PSV of 1.04 mL/g, still slightly higher than light water. LNPs with loading ratio NP1 display an average PSV of 0.935 mL/g, which is less than the PSV of light water (1.0 mL/g), causing sedimentation in light water. The PSV values for BSA (monomer at 0.68 mL/g, ~80%, and dimer at 0.66 mL/g, ~20%) are slightly lower than predicted from sequence (0.733 mL/g, as implemented in UltraScan[20]), which could be explained by hydrogen−deuterium exchange (HDX) that will occur on exposed side chains during the incubation in D_2O required for the density matching experiments. The lowest PSVs of 0.43 and 0.46 mL/g are observed for methylated and double-stranded siRNA and plasmid DNA, respectively, when sedimenting in a buffer containing 150 mM NaCl. The PSV values observed for pure nucleic acids are also lower than expected due to HDX.[21] Using the known molar mass for the siRNA (13529 Da) and the measured sedimentation and diffusion coefficients in light water buffer ($s_{20,W}$, 2.58 s; $D_{20,W}$, 9.54 cm^2/s), the calculated PSV is 0.514 mL/g for siRNA. Whenever absolute PSV values must be measured, which is not required for the purposes of this study, we recommend to substitute D_2O by $H_2{}^{18}O$. Of note, the PSV distributions of all three LNP preparations indicate a slight heterogeneity in the PSV, suggesting heterogeneity in particle size and composition (zoomed-in portion in Supporting Information Figure S1 for clarity). Figure S1 also shows that there is minimal, if any, overlap in PSV between NP6 and empty LNPs, and none with NP1, indicating that neither NP1 nor NP6 contain any measurable empty LNP components. Importantly, neither loading ratio suggests the presence of free nucleic acid, whose PSV would be <0.5 mL/g according to the siRNA and DNA density matching controls. Clear differences observed in the PSV distributions of different loadings of LNPs therefore provide a sensitive approach to compare LNP loading states. Though it is not immediately obvious why empty LNPs display a slight heterogeneity in PSV, a possible explanation is that PEG molecules, which are positioned on the surface of the LNP, are more hydrated. Since water has a higher density than the lipids on the interior of the LNP, a variation in size will therefore affect the ratio of less dense lipids in the core *vs* hydrated and therefore higher density moieties in the shell. This will affect the overall density of the particles, and therefore a mixture of differently sized empty LNPs will display a range of PSV values. Our results show clear differences in PSV for the three tested LNPs, reflecting the composition and level of nucleic acid load of these samples.

Analysis of Molar Mass and Particle Size Distributions. Once a PSV value has been determined, it is possible to derive distributions for molar mass and R_h from AUC results. Molar mass and R_h for the three LNPs are shown in Figure 2. As expected, empty LNPs exhibit the lowest molar mass and the smallest R_h of the three preparations, while NP6 and NP1 demonstrate increasing mass and R_h, respectively. Heterogeneity in the distributions is again apparent in both mass and R_h, which correlates with the heterogeneity observed in the partial specific volume (see Figure S1).

Particle sizing by cryo-TEM corroborates R_h distributions observed by AUC (see Figure 3). In each case, the cryo-TEM data suggest slightly smaller radii than those observed by AUC, which can be explained by the fact that the radii measured by cryo-TEM are based on the electron-dense regions of the particle, not on the hydrodynamic radius, which is measured by AUC or DLS (see Figure 4). The hydrodynamic radius includes the hydration layer, as well as the PEG chains, which

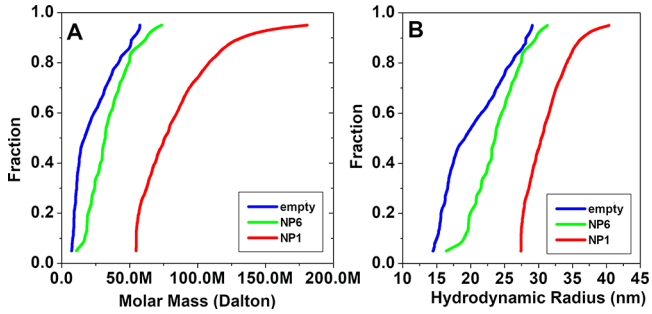

Figure 2. Molar mass distributions (A) and hydrodynamic radii distribution (B) of empty (blue), NP6 (green), and NP1 (red) LNP preparations.

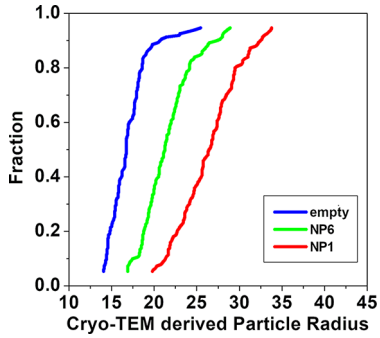

Figure 3. Cryo-TEM derived particle radii for empty LNP (blue), NP6 (green), and NP1 (red) LNPs. Total number of particles counted: 150.

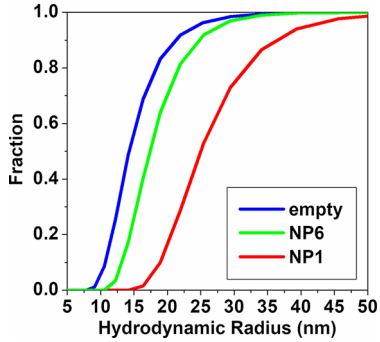

Figure 4. Number-average corrected hydrodynamic radii as measured by dynamic light scattering for empty (blue), NP6 (green), and NP1 (red) LNP preparations.

extend from the lipid core into the solvent, but have insufficient electron density to be visualized by cryo-TEM; a white ring that appears around the outside of LNPs that has been attributed to PEG lipids is actually the result of a defocused image.[22,23] The shapes of the R_h distributions of AUC and cryo-TEM differ slightly, which can be attributed to the fact that AUC does not count individual particles but is based on bulk observation and, hence, has more reliability due to better counting statistics. Whether measured by AUC or cryo-TEM, both methods produce very similar size distributions for each of the LNP formulations. However, the shape of the R_h distributions observed by DLS, while extending over the same approximate R_h range determined by AUC and cryo-TEM, appears to exaggerate the width and overemphasize larger components of the R_h distributions (see Figure 4). This can be attributed to the different scaling in DLS measurements,

https://dx.doi.org/10.1021/acsnano.0c10069
ACS Nano 2021, 15, 5068−5076

which scale with the sixth power of the particle radius, and the fact that DLS suffers from significantly lower resolution and sensitivity for heterogeneity than AUC or cryo-TEM. This suggests that DLS has limited utility for characterizing LNP formulations compared to MW-AUC.

Analysis of Multi-wavelength AUC Data. The analysis of the MW-AUC data shows that sedimentation profiles derived from the siRNA signal largely coincide with the sedimentation profiles derived from the LNP signal. This indicates that all siRNA molecules are fully complexed with lipids, in full agreement with the PSV analysis, which also did not detect siRNA free in solution. It also suggests that the NP1 and NP6 formulations do not contain empty LNPs. This was determined by spectrally separating the sedimentation distributions for the lipid and siRNA cargo components, making it possible to follow each component separately and to compare the sedimentation profiles of the spectrally separated species (LNP and siRNA in this case).[14,15] If free siRNA were present in the formulation, sedimentation profiles would diverge significantly and display positive sedimentation signals even in higher D_2O concentrations because of the significantly lower PSV of free nucleic acid (compare Figure 1). The MW-AUC data for NP1 are shown in Figure 5 and indicate that the siRNA sedimentation profile closely follows the sedimentation profile of the lipid component. The sedimentation profiles indicate a slight bias toward faster sedimentation for the lipid component over the siRNA component. It should be noted that this deviation in the sedimentation rate between the two signals is likely due to the fact that the LNP lipid shell does not absorb light, but any apparent absorbance is the result of Mie scattering. Hence, the scaling of the LNP signal is proportional to the sixth power of the shell's radius, while the siRNA absorbance is proportional to the siRNA mass, which scales only with the third power of the shell's radius. The different scalings would therefore overemphasize the larger LNP particles in the LNP signal, and small, lipid bound siRNA samples would not be visible in the LNP signal and instead be enhanced for very small particles in the spectrally separated siRNA component. This effect is most obvious with the largest LNP structures, which we observed primarily with the NP1 samples. A brief overview of the multi-wavelength AUC approach is presented in Section S2.

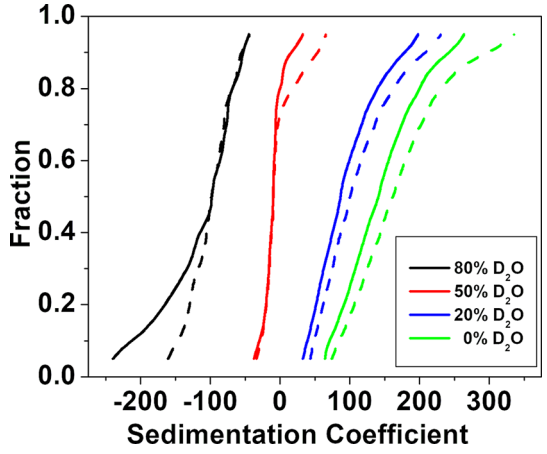

Figure 5. MW-AUC sedimentation coefficient distributions for NP1 in four different D_2O concentrations. Dashed lines represent the light-scattering signal from the lipid component, while solid lines represent the siRNA absorbance.

Validation of siRNA Incorporation in LNPs. To further validate the complete incorporation of siRNA into the LNP, we performed a separate control experiment where we measured free siRNA in the same light water buffer used for NP1 and NP6, observing a homogeneous distribution sedimenting at 2.58 s, which is in stark contrast to the sedimentation coefficient distribution observed for NP1 (ranging between ~50 and ~250 s). In a third orthogonal validation, we separately prepared NP1, formulated with fluorescently labeled siRNA, and measured it in the same light water buffer used for the unlabeled NP1 sample in an analytical ultracentrifuge equipped with a fluorescence optical system. In this experiment, only the fluorescently labeled siRNA will be detectable. The SVEs for these three experiments were analyzed by the method of van Holde–Weischet,[11] using integral sedimentation coefficient distributions. The observed distribution of the fluorescence experiment exactly matched the sedimentation distribution from the measurement of NP1 loaded with unlabeled siRNA, measured at 260 nm, proving that all siRNA must be incorporated in LNPs as predicted by the PSV and multi-wavelength experiments. These results are summarized in Figure 6.

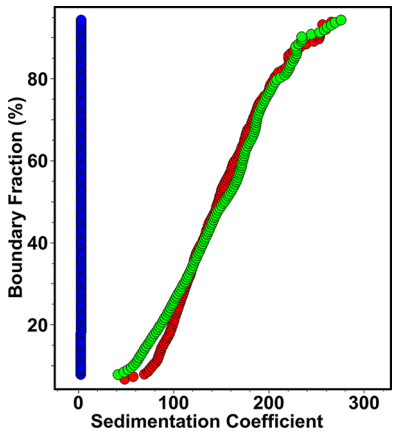

Figure 6. Validation of siRNA loading by van Holde–Weischet integral sedimentation distribution comparison between NP1 measured at 260 nm absorbance (red) and NP1 loaded with fluorescently labeled siRNA, detected by fluorescence emission (green), and pure siRNA measured by 260 nm absorbance (blue, 2.58 s).

CONCLUSIONS

We have shown that three orthogonal experimental approaches based on analytical ultracentrifugation (density matching and multi-wavelength and fluorescence emission) can be used to provide high-resolution composition information for LNP formulations and characterize LNP loading with nucleic acids. These techniques excel in terms of resolution and information content when compared to traditional methods such as light scattering or cryo-TEM, providing detailed information about LNP loading with nucleic acids. In order to distinguish loaded from empty LNPs we exploit (a) the difference in density between lipids and nucleic acids and (b) the difference in absorbance profiles between profiles from empty LNPs and from nucleic acids, and validated our results with fluorescence measurements. Our results show that density matching and

https://dx.doi.org/10.1021/acsnano.0c10069
ACS Nano 2021, 15, 5068–5076

MW-AUC can be used in tandem and extend the utility of analytical ultracentrifugation to provide reliable distributions for mass, size, and partial specific volume. We conclude that this approach represents an important alternative for the analysis of LNP formulations and can be used for routine validation of LNP formulations used for important therapeutic applications such as vaccines and gene therapy.

METHODS AND EXPERIMENT

Preparation and Analysis of Lipid Nanoparticles. LNP formulations were prepared as previously described.[19] Briefly, lipid components such as ionizable cationic lipid (KC2), distearoylphosphatidylcholine (DSPC), cholesterol, and PEG lipid were dissolved in ethanol at a ratio of 50/10/38.5/1.5 (mol %), respectively. The ethanol phase was combined with the nucleic acid aqueous phase (at pH 4) through a T-junction mixer[24,25] at a total flow rate of 20 mL/min. The resulting suspension was dialyzed against phosphate buffered saline (pH 7.4) overnight. Before AUC analysis, LNP concentrations were adjusted to range between 0.1 and 1.0 OD in the measured wavelength range. Encapsulation was determined using the RiboGreen assay.[26] Lipid content was measured using a Total Cholesterol assay kit (Wako Diagnostics, Mountain View, CA, USA), and total lipid concentration was extrapolated. LNPs were loaded with double-stranded, 21 base-pair methylated siRNA against firefly luciferase, purchased from Integrated DNA Technologies (IDT, Coralville, IA, USA).[27] Fluorescently labeled siRNA was generated by incubating RiboGreen (Invitrogen, Carlsbad, CA, USA) with siRNA prior to incorporation into LNP. The labeling ratio used was 48uL RiboGreen reagent per 1 mg of siRNA. Uncomplexed RiboGreen was removed during the overnight dialysis.

Cryogenic-Transmission Electron Microscopy. Cryo-TEM was performed as previously described.[19] A 3−5 μL drop of concentrated LNP solution was added to a glow-discharged TEM grid. A Mark IV Vitrobot (FEI, Hillsboro, OR, USA) was used to vitrify samples in liquid ethane. The frozen samples were maintained under liquid nitrogen until imaged. Imaging was performed using a FEI Tecnai LaB6 G2 TEM operating at 200 kV with a bottom-mount CCD Eagle 4k detector (FEI). Alternatively, imaging was performed on an FEI Titan Krios operating at 300 kV with a Falcon III direct electron detector. A nominal underfocus of 1 μm was used to enhance contrast. LNPs were prepared using standard rapid-mixing methods,[19] dialyzed into neutral buffer, and concentrated to achieve 15−30 mg/mL total lipid.

Analytical Ultracentrifugation. All AUC experiments were performed at the Canadian Center for Hydrodynamics at the University of Lethbridge, Alberta, Canada using an Optima AUC (Beckman Coulter). LNPs loaded with fluorescently labeled siRNA were measured in a Proteomelab XL-A (Beckman-Coulter) equipped with an Aviv fluorescence detector (excitation wavelength, 488 nm) using 3 mm titanium fluorescence assemblies (Nanolytics Instruments, Germany). All samples were measured in an An60Ti rotor, and in phosphate buffered saline and at 20 °C. Samples measured using UV-intensity optics were loaded into Epon-charcoal centerpieces and fitted with quartz windows. siRNA and plasmid DNA were measured at 260 nm, siRNA was measured at 60 krpm. and 500 scans were analyzed. Plasmid DNA was measured at 40 krpm, and 200 scans were analyzed. BSA was measured at 280 nm and 45 krpm, and 160 scans were analyzed. For LNP preparations, the rotor speed was set so that each LNP preparation provided sufficient sedimentation signal, with at least 20 scans collected per wavelength. This speed varied between D_2O concentrations and LNP preparations, and ranged between 12 and 14 krpm. All Optima AUC experiments were performed in intensity mode and analyzed with UltraScan-III, rel. 5843, as described in ref 6. MW-AUC experiments were measured between 230 and 290 nm, in 2 nm increments. SVEs are analyzed by fitting experimental data to linear combinations of finite element solutions of the Lamm equation[28] using the two-dimensional spectrum analysis (2DSA), which provides concentration distributions for the sedimentation and diffusion coefficients of each solute in a mixture.[7] LNPs are a convenient target for measuring their loading efficiency by SVE because their PSVs vary as a function of drug encapsulation due to the fact that nucleic acids are relatively dense compared to the hydrated shell (lipids and hydrated PEG molecules), resulting in a sedimenting particle that has a density close to that of light water. We describe here how the variation in PSV can be exploited by D_2O density matching experiments, and a global analysis of SVEs can be used to derive distributions that show this variation in PSV and allow us to distinguish the LNP loading state. We recall that a solute's sedimentation speed is a function of its PSV, as represented by the Svedberg relationship, shown in eq 1:

$$s = \frac{M(1 - \bar{v}\rho)}{Nf} \tag{1}$$

where s is the sedimentation coefficient, M is the molar mass, N is Avogadros number, f is the frictional coefficient, ρ is the density of the solvent, and $\bar{v}$ is the PSV of the analyte. In cases where the inverse of the buffer density equals the PSV of the particle, the buoyancy term, $1 - \bar{v}\rho$, vanishes, and no sedimentation will be observed. Therefore, by modulating the density of the solvent, it is possible to alter the sedimentation behavior of each molecule in a mixture by an amount proportional to its PSV. This effect can be exploited with a density matching experiment.[17] In this type of experiment, the density (and viscosity) of an aqueous buffer is precisely modulated by preparing the buffer with different ratios of heavy and light water, while preserving the ionic strength of the buffer.

When an analyte is sedimented in buffers with varying densities, the observed change in the sedimentation coefficient can be plotted as a function of buffer density and then extrapolated to obtain the density at $s = 0$, where $1/\rho = \bar{v}$.[29,30] When performing the experiment in a range of light and heavy water ratios, each molecule in the mixture with a different PSV will produce a different extrapolation. We exploit this phenomenon to characterize the PSV composition of a heterogeneous mixture of molecules with varying PSVs. Here, we demonstrate that replicate SVEs of LNPs, performed in buffers with different H_2O:D_2O ratios, can be used to derive the LNP loading state. Using the additional information on their spherical shape from cryo-EM experiments, we can further derive the molar mass and hydrodynamic radius.

By performing the experiment in multi-wavelength mode (scanning between 230 and 290 nm with 2 nm increments), it is possible to optically resolve the contributions from the lipids and the nucleic acids, since they differ in their spectral contributions over the examined spectral range (detailed descriptions of the MW-AUC method can be found in the literature;[14−16,31] an introductory explanation of the method is provided in Section S2). Nucleic acids produce a characteristic 260 nm absorbance band, while the lipid nanoparticles do not absorb at all, but instead display a characteristic Mie-scattering profile with a monotonically increasing absorbance signal with decreasing wavelength (see Figure 7). Capitalizing on these spectral differences, it is possible to resolve siRNA signal from lipid signal by using a non-negatively constrained least-squares

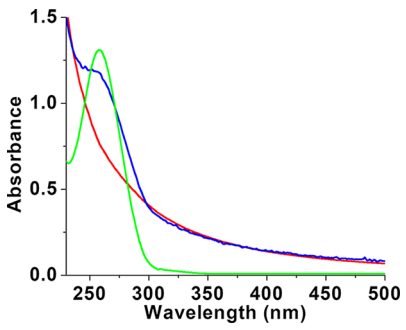

Figure 7. UV spectral properties of RNA (green), empty LNP (red), and RNA-loaded LNPs (blue).

https://dx.doi.org/10.1021/acsnano.0c10069
ACS Nano 2021, 15, 5068−5076

decomposition of the wavelength scans obtained in the multi-wavelength experiment and analyze their hydrodynamic properties separately. By examining sedimentation coefficient distributions for each signal separately, it is possible to determine if the two molecules co-sediment as a single particle with identical sedimentation coefficients, in which case the siRNA is encapsulated by the liposome, or if the RNA is free in solution. In the latter case, their sedimentation and PSV distributions would be significantly different because of the buoyancy differences. We have developed an algorithm capable of combining all analysis steps required to deduce distributions for the partial specific volume, and implemented it in a module (termed *us_buoyancy*) that is now part of the UltraScan software suite.[20] UltraScan is a multiplatform, open source software that can be freely downloaded from our Web site (http://ultrascan3.aucsolutions.com). Our approach employs the following steps:

1. For a density matching experiment, an equal amount of LNP sample is diluted into phosphate buffered saline, pH 7.4, prepared in four different ratios of H_2O:D_2O ranging between 0% and 99% D_2O. In order to achieve conditions with high D_2O content, it is recommended to prepare buffers in D_2O directly and to dilute a highly concentrated LNP sample with the D_2O buffer to minimize the amount of light water in the final sample. It is important to maintain the same analyte concentration in each replicate experiment to avoid mass action effects, which could alter the sedimentation coefficient distribution. To obtain a 20× D_2O buffer stock solution, we prepared a 20× buffer in light water, dried an aliquot in a lyophilizer, and resuspended the pellet in D_2O to create 20× D_2O buffer. An assumption is made that the LNPs do not change chemically in response to variable D_2O concentrations and maintain their assembly state composition. Whenever D_2O is employed, the potential for HDX exists, which affects the absolute PSV measured with variable effect on different macromolecules, with nucleic acids and proteins more sensitive to HDX than aliphatic groups in lipids.[22,32] Investigators concerned with the impact of HDX on the PSV can substitute D_2O with the significantly more expensive $H_2{}^{18}O$, which has physical properties similar to those of D_2O, but avoids deuterium exchange artifacts.

2. In general, it is preferable to perform the sedimentation velocity experiments at low enough sample concentrations to maintain near ideal transport behavior but high enough to still produce sufficient signal across the examined wavelength range, utilizing the full dynamic range of the detector. Rotor speeds should be fast enough to optimize sedimentation separation of solutes, while at the same time slow enough to obtain sufficient scan numbers. For multi-wavelength sedimentation velocity experiments in the Optima AUC instrument, it is recommended to use a speed that synchronizes the lamp's flash rate with the rotor speed; this will minimize scanning time and allow a sufficient number of scans to be recorded for each wavelength before the sample is pelleted. For LNPs investigated at the Canadian Center for Hydrodynamics this condition is matched at speeds between 12,000 and 14,000 rpm, which results in a 19−17 s scan time, respectively, for both cell channels.

3. Each experimental data set is analyzed according to standard workflows implemented in UltraScan to derive an iterative two-dimensional spectrum analysis (2DSA) model for each triple,[7] which is defined to be the data resulting from one cell, one channel, and a single wavelength. Our approach includes a stepwise refinement of the fit by first removing time-invariant noise contributions from the data and then adding removal of radially invariant noise contributions, and to fit the meniscus and cell bottom positions. Finally, an iterative refinement of the two-dimensional parameter space is performed. Additional refinement by the 2DSA-Monte Carlo analysis[8] or the parametrically constrained spectrum analysis[5] is recommended when additional regularization is needed. The 2DSA method requires the generation of a grid that spans the parameter space of the sedimentation and diffusion coefficients describing the experimental system. This grid typically uses a parametrized grid based on the sedimentation coefficient and the frictional ratio, φ, describing the anisotropy of each species.[1] The parametrization of the diffusion coefficient using φ requires an initial guess of the value of the PSV, which is typically assumed to be constant for all species to be fitted, or bimodal for experiments which contain both sedimenting and floating solutes. It is important to note that even if the actual values of the PSV differ, the grid can nevertheless accurately represent the appropriate sedimentation and diffusion coefficients, as long as the frictional ratio φ covers all sedimentation and diffusion coefficients needed to explain the experimental data. Whether this condition is met can be assessed by the RMSD and the randomness of the residuals produced in the fit. Hence, accurate values for the PSV are not needed *a priori* to obtain a satisfactory fit of the experimental data. In UltraScan, conversion of observed sedimentation and diffusion coefficients to standard conditions (based on buffer viscosity, density, and experimental temperature) is automatically performed, producing models composed of multiple discrete species, where each species is represented by a $s_{20,W}$ value, a $D_{20,W}$ value, and a partial concentration. For this application it is important that the density increment due to D_2O is not added to the buffer correction, since the effect of the density variation contributed by D_2O is used to globally obtain PSV distributions. However, viscosity corrections due to the addition of D_2O must be included. Examples for such plots obtained for LNP preparations containing two different loading ratios are shown in Figure 8.

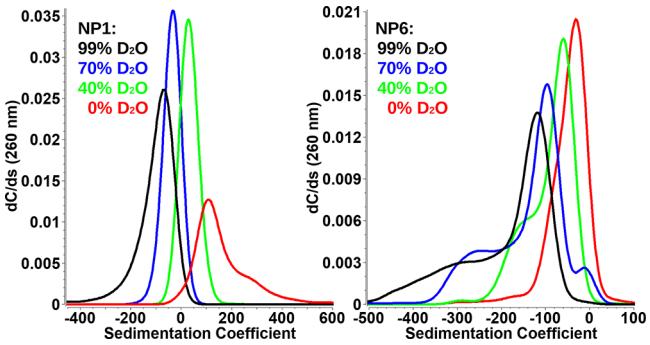

Figure 8. Sedimentation coefficient distributions for density matching SVEs of two different LNP loading ratios (phospholipid:RNA backbone phosphate). NP1, containing one phospholipid molecule per siRNA phosphate is shown on the left; NP6, containing six phospholipid molecules per siRNA phosphate is shown on the right. Distributions are shown for four buffers containing 0−99% D_2O (0%, red; 40%, green; 70%, blue; 99%, black).

4. Integral distributions for sedimentation and diffusion coefficients, based on the hydrodynamically corrected values, are derived from the final model distributions obtained in item 3, where the diffusion coefficient (D) is given by

$$D = \frac{RT}{Nf} \tag{2}$$

where R is the universal gas constant and T is the temperature in kelvin. Like s, D is inversely proportional to the frictional properties of the molecule. Diffusion distributions ($D_{20,W}$) from all D_2O concentrations can be averaged across measurements from all buffers but only for values taken from identical boundary fractions. Since diffusion is only affected by viscosity, a value that is already corrected, no further correction needs to be applied to the diffusion values measured from different buffers. Also, since the analyte concentration is held constant, equivalent boundary fractions correspond to the same sedimenting species across all buffer densities. Since the analyte concentration in each D_2O concentration sample is identical, integral distributions will reflect the same sample concentration and can therefore be normalized to account for minor variations in cell pathlengths. Examples of integral sedimentation coefficient distributions for NP6 LNPs in different H_2O:D_2O mixtures are shown in Figure 9. Boundary fractions near the extremes (5−10%) are sensitive

https://dx.doi.org/10.1021/acsnano.0c10069
ACS Nano 2021, 15, 5068−5076

to experimental noise and therefore tend to be less reliable and are typically excluded from the plots.

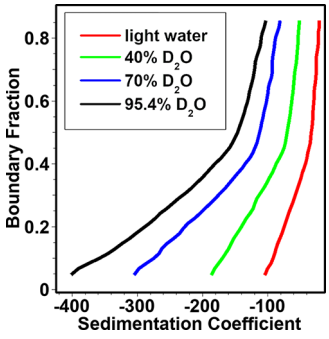

Figure 9. Integral sedimentation coefficient distributions for NP6 in four different D_2O concentrations (0%, red; 40%, green; 70%, blue; 95.4%, black).

5. For each corresponding boundary fraction from each buffer, the corresponding viscosity-corrected s values and $D_{20,W}$ values are recorded. The s values are now plotted against the density of each buffer and extrapolated to the zero sedimentation point. The density of the solution at the zero sedimentation point represents the density where the species in this boundary fraction is exactly buoyant in the buffer solution. The inverse of this density equals the PSV of the sample, and since each boundary fraction can extrapolate to a different position, this procedure generates a unique partial specific volume for each boundary fraction. The collection of all extrapolated boundary fractions represents the PSV distribution for the mixture.

6. Using the boundary fraction arrays for the PSV, and the $s_{20,W}$ and $D_{20,W}$ values obtained in light water, additional properties of the sample composition can now be derived numerically. Combining and rearranging eqs 1 and 2 directly yield the molar mass:

$$M = \frac{sRT}{D(1 - \bar{\nu}\rho)} \tag{3}$$

The frictional coefficient of each particle can be obtained from the diffusion coefficient:

$$f = \frac{RT}{ND} \tag{4}$$

Combining this result with the Stokes–Einstein relationship, the hydrodynamic radius, R_h, can be obtained:

$$R_h = \frac{f}{6\pi\eta} \tag{5}$$

where η signifies the viscosity of the solvent. Representing the volume of each particle as a perfect sphere, the minimal radius, R_0, of each particle (eq 6) and the corresponding frictional coefficient, f_0, can be derived from the Stokes–Einstein relationship (eq 7):

$$R_0 = \left(\frac{3M\bar{\nu}}{4\pi N}\right)^{1/3} \tag{6}$$

$$f_0 = 6\pi\eta R_0 \tag{7}$$

Finally, the anisotropy, φ, or frictional ratio, of the particle can be obtained:

$$\varphi = \frac{f}{f_0} \tag{8}$$

Screenshots of the UltraScan module dialogues used to generate distributions from these parameters and display them as integral distribution graphs are shown in Figures S4 and S5.

In some cases, additional constraints can be applied.[4] For LNPs, cryo-TEM results suggest the presence of mostly spherical particles (see Figure 10). If particles are spherical as confirmed by a separate technique such as cryo-TEM, the assumption can be made that φ (eq 8) for most particles corresponds to an anisotropy of unity. This is helpful in cases where the diffusion signal is weak, either because the sedimentation is too fast, not allowing enough time for sufficient diffusion signal to be collected, or the heterogeneity is so large that the signal of the diffusion coefficient for individual species is simply too small to be of any value. In the case of LNPs examined here, both conditions apply, and an additional constraint based on the anisotropy allows us to calculate the appropriate diffusion coefficient by transforming the sedimentation and PSV data pairs with eq 9, using $\varphi = 1.0$:

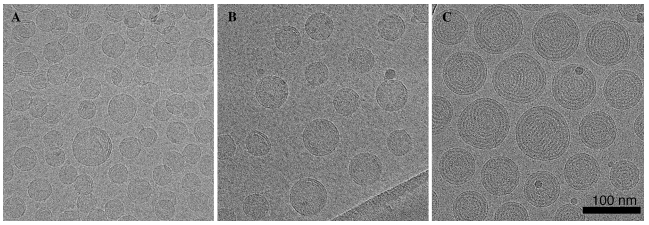

Figure 10. Cryo-TEM images of empty LNP (A), NP6 filled LNPs (B), and NP1 filled LNPs (C) suggesting the presence of mostly spherical particles, regardless of loading stage, justifying the use of the anisotropy constraint $\varphi = 1.0$.

$$D = \frac{RT}{9\pi\eta\varphi N}\left(\frac{2s\varphi\bar{\nu}\eta}{1 - \bar{\nu}\rho}\right)^{-0.5} \tag{9}$$

This constraint can be incorporated into the fitting equation and tested for validity by confirming random residuals for the fitted data. To further validate our assumption of $\varphi = 1.0$, we offer the following observations: Even though the actual hydration layer, including PEG molecules, cannot be observed by cryo-TEM, it is reasonable to expect that the hydration layer does not substantially alter the morphology of LNPs and that it simply replicates the spherical shape observed in the cryo-TEM images (see Figure 10). Furthermore, simulations with φ values larger than unity yield hydrodynamic radii no longer consistent with the DLS measurements of the hydrodynamic radius. We show an example of predictions for hydrodynamic radius and molar mass based on higher anisotropies ($\varphi = 1.2$, $\varphi = 1.5$) in Figure S6.

LIMITATIONS

We noticed that for heterogeneous samples the density matching algorithm is very sensitive to the absorbance baseline determined while deriving the time-invariant noise during fitting.[33] When baselines did not precisely align between SVEs performed in different buffers, any larger steps in partial specific volume for different molecular mixtures, for example, mixtures of non-interacting proteins and DNA, can cause slight shifts in boundary fractions, no longer guaranteeing a precise alignment of solutes represented in specific boundary fractions. This can cause erratic extrapolations in the transition region of the boundary fractions, which can be avoided by lowering the number of divisions along the boundary. Also, the problem can be minimized by carefully fitting the original SVEs, making sure that any buffer absorbance is properly accounted for in the time-invariant noise component, leading to a zero baseline for all data sets included in the density matching extrapolation.

ASSOCIATED CONTENT

Supporting Information

The Supporting Information is available free of charge at https://pubs.acs.org/doi/10.1021/acsnano.0c10069.

https://dx.doi.org/10.1021/acsnano.0c10069
ACS Nano 2021, 15, 5068–5076

(Figure S1) Zoom-in of the partial specific volume plot shown in Figure 1; Section S2: multi-wavelength analytical ultracentrifugation method; (Figure S3) single multi-wavelength Optima AUC scan; (Figure S4) UltraScan dialogue for entering the D_2O percentages; (Figure S5) main screen of the UltraScan us_buoyancy module; (Figure S6) hydrodynamic radius and molar mass predictions (PDF)

AUTHOR INFORMATION

Corresponding Author

Borries Demeler − *Department of Chemistry and Biochemistry, The University of Lethbridge, Lethbridge, Alberta, Canada T1K 3M4; AUC Solutions, Houston, Texas 77494, United States; Department of Chemistry, University of Montana, Missoula, Montana 59812, United States;* orcid.org/0000-0002-2414-9518; Email: demeler@gmail.com

Authors

Amy Henrickson − *Department of Chemistry and Biochemistry, The University of Lethbridge, Lethbridge, Alberta, Canada T1K 3M4;* orcid.org/0000-0003-3266-5202

Jayesh A. Kulkarni − *Department of Biochemistry and Molecular Biology, Faculty of Medicine, University of British Columbia, Vancouver, British Columbia, Canada V6T 1Z3;* orcid.org/0000-0002-3622-6998

Josh Zaifman − *Department of Biochemistry and Molecular Biology, Faculty of Medicine, University of British Columbia, Vancouver, British Columbia, Canada V6T 1Z3*

Gary E. Gorbet − *AUC Solutions, Houston, Texas 77494, United States*

Pieter R. Cullis − *Department of Biochemistry and Molecular Biology, Faculty of Medicine, University of British Columbia, Vancouver, British Columbia, Canada V6T 1Z3;* orcid.org/0000-0001-9586-2508

Complete contact information is available at: https://pubs.acs.org/10.1021/acsnano.0c10069

Author Contributions

A.H. performed AUC experiments and analyzed AUC data, plus edited the manuscript. J.A.K. synthesized LNP particles, performed cryo-TEM experiments and data analysis, and edited the manuscript. (A.H. and J.A.K. contributed equally to this work.) G.E.G. coded the density matching algorithm module and the multi-wavelength module in the UltraScan software. J.Z. synthesized the lipids used in the LNP formulations. P.R.C. was responsible for conceptualization and funding. B.D. additional contributed to conceptualization, analyzed data, wrote the manuscript, and secured funding. All authors contributed to the editing of the manuscript.

Notes

The authors declare no competing financial interest.

The UltraScan software including the new density matching module can be freely downloaded from https://ultrascan3.aucsolutions.com/download.php.

ACKNOWLEDGMENTS

This work was supported by the Canada 150 Research Chairs program (Grant C150-2017-00015), the Canada Foundation for Innovation (Grant CFI-37589), the National Institutes of Health (Grant 1R01GM120600), and the Canadian Natural Science and Engineering Research Council (Grant DG-RGPIN-2019-05637). All grants are issued to B.D. UltraScan supercomputer calculations were supported through NSF/XSEDE Grant TG-MCB070039N (to B.D.) and University of Texas Grant TG457201 (to B.D.). Computational resources and support from the University of Montana's Griz Shared Computing Cluster (GSCC) contributed to this research. P.R.C. is funded by a Foundation Grant (FDN 148469) from the Canadian Institutes of Health Research. J.A.K. is supported (in part) by a postdoctoral fellowship from NanoMedicines Innovation Network (NMIN), a member of the Networks of Centers of Excellence Canada program. P.R.C. is the scientific director and awardee of NMIN, including two grants (2019-NC-01 and 2019-T2-01). We thank Marc Roussel for critically reading our manuscript.

REFERENCES

(1) Kim, H.; Brookes, E.; Cao, W.; Demeler, B. Two-Dimensional Grid Optimization for Sedimentation Velocity Analysis in the Analytical Ultracentrifuge. *Eur. Biophys. J.* **2018**, *47* (7), 837−844.

(2) Williams, T. L.; Gorbet, G. E.; Demeler, B. Multi-Speed Sedimentation Velocity Simulations with UltraScan-III. *Eur. Biophys. J.* **2018**, *47* (7), 815−823.

(3) Gorbet, G. E.; Mohapatra, S.; Demeler, B. Multi-Speed Sedimentation Velocity Implementation in UltraScan-III. *Eur. Biophys. J.* **2018**, *47* (7), 825−835.

(4) Demeler, B.; Nguyen, T. L.; Gorbet, G. E.; Schirf, V.; Brookes, E. H.; Mulvaney, P.; El-Ballouli, A. O.; Pan, J.; Bakr, O. M.; Demeler, A. K.; Hernandez Uribe, B. I.; Bhattarai, N.; Whetten, R. L. Characterization of Size, Anisotropy, and Density Heterogeneity of Nanoparticles by Sedimentation Velocity. *Anal. Chem.* **2014**, *86* (15), 7688−95.

(5) Gorbet, G.; Devlin, T.; Hernandez Uribe, B.; Demeler, A. K.; Lindsey, Z.; Ganji, S.; Breton, S.; Weise-Cross, L.; Lafer, E. M.; Brookes, E. H.; Demeler, B. A Parametrically Constrained Optimization Method for Fitting Sedimentation Velocity Experiments. *Biophys. J.* **2014**, *106*, 1741−50.

(6) Demeler, B. Methods for the Design and Analysis of Sedimentation Velocity and Sedimentation Equilibrium Experiments with Proteins. *Cur. Protoc. Prot. Sci.* **2010**, *60*, 1−31.

(7) Brookes, E.; Cao, W.; Demeler, B. A Two-Dimensional Spectrum Analysis for Sedimentation Velocity Experiments of Mixtures with Heterogeneity in Molecular Weight and Shape. *Eur. Biophys. J.* **2010**, *39* (3), 405−14.

(8) Demeler, B.; Brookes, E. Monte Carlo Analysis of Sedimentation Experiments. *Colloid Polym. Sci.* **2008**, *286* (2), 129−137.

(9) Brookes, E.; Demeler, B. Parallel Computational Techniques for the Analysis of Sedimentation Velocity Experiments in UltraScan. *Colloid Polym. Sci.* **2008**, *286* (2), 139−148.

(10) Brookes, E.; Demeler, B. Parsimonious Regularization Using Genetic Algorithms Applied to the Analysis of Analytical Ultracentrifugation Experiments. *GECCO '07 Proceedings of the 9th Annual Conference on Genetic and Evolutionary Computation*, July 7−11, 2007, London, England; Association for Computing Machinery (ACM): New York, 2007; pp 361−368, DOI: 10.1145/1276958.1277035.

(11) Demeler, B.; van Holde, K. E. Sedimentation Velocity Analysis of Highly Heterogeneous Systems. *Anal. Biochem.* **2004**, *335* (2), 279−288.

(12) Cao, W.; Demeler, B. Modeling Analytical Ultracentrifugation Experiments with an Adaptive Space-Time Finite Element Solution for Multi-Component Reacting Systems. *Biophys. J.* **2008**, *95* (1), 54−65.

(13) Cao, W.; Demeler, B. Modeling Analytical Ultracentrifugation Experiments with an Adaptive Space-Time Finite Element Solution of the Lamm Equation. *Biophys. J.* **2005**, *89* (3), 1589−602.

(14) Zhang, J.; Pearson, J. Z.; Gorbet, G. E.; Cölfen, H.; Germann, M. W.; Brinton, M. A.; Demeler, B. Spectral and Hydrodynamic Analysis of West Nile Virus RNA-Protein Interactions by Multi-wavelength Sedimentation Velocity in the Analytical Ultracentrifuge. *Anal. Chem.* **2017**, *89* (1), 862−870.
(15) Gorbet, G. E.; Pearson, J. Z.; Demeler, A. K.; Cölfen, H.; Demeler, B. Next-Generation AUC: Analysis of Multiwavelength Analytical Ultracentrifugation Data. *Methods Enzymol.* **2015**, *562* (1), 27−47.
(16) Pearson, J. Z.; Krause, F.; Haffke, D.; Demeler, B.; Schilling, K.; Cölfen, H. Next-Generation AUC Adds a Spectral Dimension. *Methods Enzymol.* **2015**, *562* (1), 1−26.
(17) Swygert, S. G.; Manning, B. J.; Senapati, S.; Kaur, P.; Lindsay, S.; Demeler, B.; Peterson, C. L. Solution-State Conformation and Stoichiometry of Yeast Sir3 Heterochromatin Fibres. *Nat. Commun.* **2014**, *5*, 4751.
(18) Kulkarni, J. A.; Witzigmann, D.; Chen, S.; Cullis, P. R.; van der Meel, R. Lipid Nanoparticle Technology for Clinical Translation of siRNA Therapeutics. *Acc. Chem. Res.* **2019**, *52* (9), 2435−2444.
(19) Kulkarni, J. A.; Darjuan, M. M.; Mercer, J. E.; Chen, S.; van der Meel, R.; Thewalt, J. L.; Tam, Y. Y. C.; Cullis, P. R. On the Formation and Morphology of Lipid Nanoparticles Containing Ionizable Cationic Lipids and siRNA. *ACS Nano* **2018**, *12* (5), 4787−4795.
(20) Demeler, B., Gorbet, G. Analytical Ultracentrifugation Data Analysis with UltraScan-III. In *Analytical Ultracentrifugation: Instrumentation, Software, and Applications*; Uchiyama, S., Stafford, W. F., Laue, T., Eds.; Springer: Tokyo, Japan, 2016; Chapter 8, pp 119−143, DOI: 10.1007/978-4-431-55985-6_8.
(21) Largy, E.; Gabelica, V. Native Hydrogen/Deuterium Exchange Mass Spectrometry of Structured DNA Oligonucleotides. *Anal. Chem.* **2020**, *92* (6), 4402−4410.
(22) Murata, K.; Wolf, M. Cryo-Electron Microscopy for Structural Analysis of Dynamic Biological Macromolecules. *Biochim. Biophys. Acta, Gen. Subj.* **2018**, *1862* (2), 324−334.
(23) Franken, L. E.; Boekema, E. J.; Stuart, M. C. A. Transmission Electron Microscopy as a Tool for the Characterization of Soft Materials: Application and Interpretation. *Adv. Sci. (Weinh).* **2017**, *4* (5), 1600476.
(24) Jeffs, L.; Palmer, L.; Ambegia, E.; Giesbrecht, C.; Ewanick, S.; MacLachlan, I. A Scalable, Extrusion-Free Method for Efficient Liposomal Encapsulation of Plasmid DNA. *Pharm. Res.* **2005**, *22*, 362−372.
(25) Kulkarni, J. A.; Tam, Y. Y. C.; Chen, S.; Tam, Y. K.; Zaifman, J.; Cullis, P. R.; Biswas, S. Rapid Synthesis of Lipid Nanoparticles Containing Hydrophobic Inorganic Nanoparticles. *Nanoscale* **2017**, *9* (36), 13600−13609.
(26) Chen, S.; Tam, Y. Y.; Lin, P. J.; Leung, A. K.; Tam, Y. K.; Cullis, P. R. Development of Lipid Nanoparticle Formulations of siRNA for Hepatocyte Gene Silencing Following Subcutaneous Administration. *J. Controlled Release* **2014**, *196*, 106−12.
(27) Basha, G.; Ordobadi, M.; Scott, W. R.; Cottle, A.; Liu, Y.; Wang, H.; Cullis, P. R. Lipid Nanoparticle Delivery of siRNA to Osteocytes Leads to Effective Silencing of SOST and Inhibition of Sclerostin *in Vivo*. *Mol. Ther.–Nucleic Acids* **2016**, *5* (9), No. e363.
(28) Lamm, O. Die Differentialgleichung der Ultrazentrifugierung. *Ark. Mater. Astron. Fys.* **1929**, *21B*, 1−4.
(29) Edelstein, S. J.; Schachman, H. K. Measurement of Partial Specific Volume by Sedimentation Equilibrium in H_2O-D_2O Solutions. *Methods Enzymol.* **1973**, *27*, 82−98.
(30) Gohon, Y.; Pavlov, G.; Timmins, P.; Tribet, C.; Popot, J. L.; Ebel, C. Partial Specific Volume and Solvent Interactions of Amphipol A8−35. *Anal. Biochem.* **2004**, *334* (2), 318−34.
(31) Demeler, B. Measuring Molecular Interactions in Solution Using Multi-Wavelength Analytical Ultracentrifugation: Combining Spectral Analysis with Hydrodynamics. *Biochemist (London)* **2019**, *41* (2), 14−18.
(32) Breyton, C.; Gabel, F.; Lethier, M.; Flayhan, A.; Durand, G.; Jault, J. M.; Juillan-Binard, C.; Imbert, L.; Moulin, M.; Ravaud, S.; Härtlein, M.; Ebel, C. Small Angle Neutron Scattering for the Study of Solubilised Membrane Proteins. *Eur. Phys. J. E: Soft Matter Biol. Phys.* **2013**, *36*, 71.
(33) Schuck, P.; Demeler, B. Direct Sedimentation Boundary Analysis of Interference Optical Data in Analytical Ultracentrifugation. *Biophys. J.* **1999**, *76*, 2288−2296.

https://dx.doi.org/10.1021/acsnano.0c10069
ACS Nano 2021, 15, 5068−5076